AIAA JOURNAL
Vol. 34, No. 5, May 1996

Numerical Simulations of Flow Modification of Supersonic Rectangular Jets

Ronald Kolbe,* Kazhikathra Kailasanath,† Theodore Young,‡ Jay Boris,§ and Alexandra Landsberg¶
U.S. Naval Research Laboratory, Washington, D.C. 20375-5344

Numerical simulations have been performed to study the flowfield and near-field noise of a supersonic rectangular jet with two paddles inserted into the flow. The paddles cause a strong flapping motion to develop that enhances mixing of the jet with the surroundings. These simulations have been used to determine the flapping motion's frequency, the mixing enhancement, the near-field noise, and the thrust loss associated with the paddles and to study the acoustic feedback mechanism that modulates the flapping motion. The flapping frequency has been estimated using the pitot pressure distributions at a sequence of times and Fourier analysis of the local pressure and z component of velocity. For paddles located $x/h = 7.3$ from the nozzle, where h is the narrow dimension of the nozzle, a frequency of 4700 Hz [$St(h) = 0.136$] with an amplitude of 157.5 dB at the nozzle lip has been predicted and is in agreement with experimental results. The pitot pressure drop, the mass, and the x-momentum fluxes along the flow direction have been used as a measure of jet mixing for jets with and without paddles inserted into the flow. In our numerical simulations, a control volume approach was used to estimate the thrust loss caused by the insertion of the paddles. The computational value of 13% is close to the experimental value of 14.4%, considering that the physical support for the paddles in the experiments is not included in the simulations. A special sequence of local pressure distribution plots, which highlight the acoustic waves, has been used to study the feedback mechanism that modulates the flapping motion.

Introduction

THE noise generated by the engines of military airplanes and the proposed high-speed civil transport (HSCT) is a major environmental concern. Although there are many sources, a major contribution to the noise comes from the jet exhausts. To control and reduce this noise, experimental evidence suggests that various flow modification methods can enhance jet mixing and noise control. These modification methods include the effect of pressure waves,[1,2] acoustic excitation,[3] the role of tabs,[4,5] counterflowing nozzles,[6] and paddles.[7] Rice and Raman[7] have demonstrated experimentally that immersion of two obstacles (called paddles) on either side of a rectangular jet and parallel to the jet's major axis and perpendicular to the flow can generate an intense flapping motion of the jet, which appears to significantly enhance its mixing with the surroundings. As an adjunct to these flow modifications some loss to the thrust is also to be expected.

Theoretical and experimental studies, including Lighthill,[8] Powell et al.,[9] Tam,[10] and Tam and Ahuja,[11] have shown that noise is generated in the shear layer of the jet and that external acoustical sources and impingement tones can modify and trigger instabilities here. It is, therefore, believed that the effect of the paddles is to generate an impingement tone that propagates upstream along the outside of the jet in the subsonic flow and excites the flapping mode of the jet. This sets up a resonant self-sustaining loop.[7] The rapid flapping motion of the jet results in an increase in the acoustic screech at the jet exit. However, this increase is not thought to be a major problem because screech can be absorbed by the use of acoustic liners in the ejector. Of greater concern is the thrust loss caused by the immersion of the paddles in the jet exhaust. Numerical simulations are a valuable tool both in expanding our fundamental understanding of various mechanisms of mixing enhancement and flow excitation and in performing design optimization studies.

In this paper, we report on the application of numerical simulations to investigate the role of paddles in enhancing the mixing of supersonic rectangular jets. In the next section, we briefly discuss the flow configuration simulated and the numerical model. We discuss studies that have been performed to show that the dominant frequency and amplitude of the flapping motion are not affected by the choice of the grid and the computational domain. Then we present two simulations, a free jet and a jet with paddles immersed in the flow. The two simulations are compared to show the effects of the paddles. Various computational diagnostics have been developed to improve understanding of the flow. These include frequency analysis and measures of mixing enhancement and thrust loss caused by the paddles. Finally, we compare our results to observations from the experiments of Rice and Raman.[7]

Numerical Simulation Model

Physical Problem

The numerical simulation models a rectangular supersonic jet with and without long square cross-sectional paddles inserted parallel to the jet's major axis and perpendicular to the flow (Fig. 1). The rectangular nozzle is 1.4 × 6.86 cm, with an aspect ratio of 4.9. The square paddles are 0.32 × 0.32 and 7.6 cm in length. For the experiment simulated (or the case simulated), the paddles are located 10.16 cm from the nozzle exit plane to the paddle's front and 0.6 cm from the jet's major axis to the paddle's side. Therefore, the paddles are immersed approximately 0.1 cm into the jet flow. The location of the paddles from both the nozzle's exit plane and major axis can be varied within the computational model. Only perfectly expanded jets are considered in this paper.

Computational Model

The computations are performed using the simulation program called FAST3D, which solves the unsteady conservation equations for mass, momentum, and energy in three dimensions using the flux-corrected transport (FCT) algorithm.[12] The FCT algorithm was designed to solve generalized continuity equations for space and time-varying coordinates. For the results reported in this paper, the

Presented as Paper 95-0725 at the AIAA 33rd Aerospace Sciences Meeting and Exhibit, Reno, NV, Jan. 9–12, 1995; received July 31, 1995; revision received Dec. 4, 1995; accepted for publication Dec. 19, 1995.

*Mechanical Engineer, Laboratory of Computational Physics and Fluid Dynamics, Code 6410. Member AIAA.
†Head, Center for Reactive Flow and Dynamical Systems, Code 6410. Associate Fellow AIAA.
‡Research Physicist, Laboratory for Computational Physics and Fluid Dynamics, Code 6440.
§Chief Scientist and Director, Laboratory for Computational Physics and Fluid Dynamics, Code 6400. Fellow AIAA.
¶Aerospace Engineer, Laboratory for Computational Physics and Fluid Dynamics, Code 6410. Member AIAA.

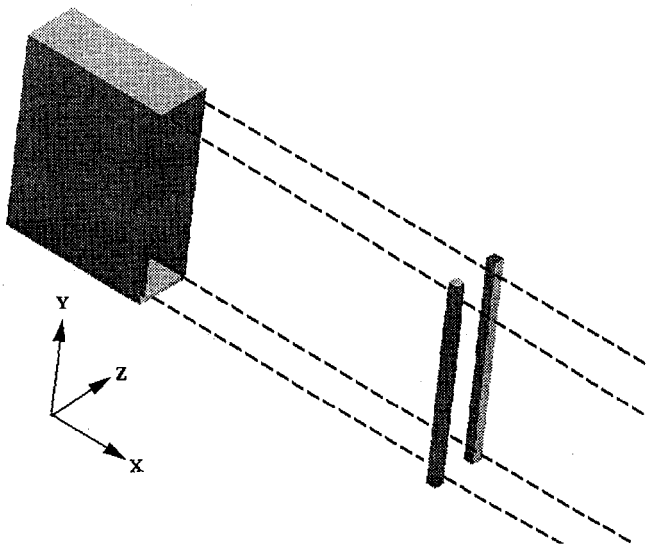

Fig. 1 Rectangular nozzle and paddles.

most recent version of the algorithm, which is fourth-order accurate in space in smooth regions of the flow and second-order accurate in time.[13] The FCT algorithm is well tested, monotone (positivity preserving), and conservative. Monotonicity is achieved by introducing a diffusive flux modified by a flux limiter. In the code FAST3D, FCT is used along with the virtual-cell embedding (VCE)[14] technique to simulate flows over arbitrarily complex objects.[15,16]

The VCE method was developed to resolve complex geometries on a structured, orthogonal grid with little sacrifice in speed or memory. An orthogonal, structured, rectilinear mesh is used, but variable spacing between the grid planes and even motion of the grid planes are allowed. With the VCE method, cells may be fully outside the body, fully inside the body, or partitioned by the body. It is these partitioned, boundary cells that require special treatment. The VCE method computes partial volumes and partial face areas for all of the cells that intersect the body. Thus, this approach only refines (subdivides) cells next to the body. CPU time is not sacrificed appreciably since only those cells next to the body require special treatment. The term "virtual" is used since the subcells embedded within a cell are not stored in memory and therefore are not integrated in the solution.

FAST3D was originally developed on a serial-vector computer, but the evolution of less expensive parallel computers provided an opportunity to develop a cost-effective version of FAST3D capable of running large-grid, long-duration (50,000 time steps or more) simulations in relatively short times. To preserve much of the original code and its long vector features, an efficient running-transpose (RT) data structure is employed. A virtual node system is incorporated to simplify the transpose on varying numbers of physical (computational) nodes, to permit a change in the number of actual physical nodes in midsimulation, and to provide fault tolerance for the very long run times required. By preserving much of the original code, simulations with very complex geometry can be initialized on more easily programmable serial computers and the results can be analyzed off line by sharing dump/restart files.

Computational Domain

Since the dominant mode of flapping is along the minor axis, we used a plane of symmetry formed by the jet's minor axis (the z direction) and the direction of jet flow (the x direction). Thus, the computational domain contains only the upper half of the flowfield. This domain was chosen to reduce the computational run time and storage requirements and was resolved by a structured, stretched rectilinear grid. The coordinate directions were defined as follows: the x direction is the direction of jet flow; the y direction is the nozzle's major axis (long width); and the z direction is the nozzle's minor axis (short width, see Fig. 1). The nozzle's rigid, thin walls are modeled (in most cases) by making the interface between two adjacent cells impregnable to the flow. The computational domain boundaries are located far enough from the major flow features using a stretched grid to minimize unphysical pressure waves being reflected back into the domain. The regular grid region surrounding the nozzle and paddles is sufficiently large to allow the propagation of the waves from the paddles to the nozzle to be well resolved. This regular grid region, which resolves the hydrodynamics is approximately from 0.0 to 16.6 cm in the x direction, 0.0 to 4 cm in the y direction, and ± 2.5 cm in the z direction. To initiate the flow, an impulsively started, fully expanded supersonic jet issues from the rectangular nozzle.

Computational Resolution Studies

The flapping motion of the jet is the dominant feature observed in the simulations discussed in this paper. Since a perfect grid and computational domain do not exist, various changes to the grid resolution and computational domain (as discussed earlier) were studied for their effect on the flapping motion's dominant frequency. These grids were not chosen to resolve completely all issues but to ensure that the present studies had converged and to place some limits on the grid effects on the solutions. Four different grids have been used. The first grid used, $120 \times 80 \times 80$, was chosen to minimize run time and to provide preliminary results. The second grid, $120 \times 104 \times 104$, increased the computational domain and grid resolution. The third grid, $120 \times 104 \times 120$, extended the computational domain in the z direction, the direction of the flapping motion, and was used for most simulations and all those presented in this paper. Within the regular grid region, the spacings for the grid were $\Delta x = 0.2$, $\Delta y = 0.07$, and $\Delta z = 0.07$ cm. A fourth grid, 120112×136, extended the computational domain in the z and y directions to further resolve grid issues.

The dominant frequency varied 5% of $St(h) = 0.136$ for the various domains and grid spacing tried. The Strouhal number $St(h)$ is defined as fh/U_j where f is the frequency, h is the narrow nozzle dimension of 1.4 cm, and U_j is the jet exit velocity of 4.833×10^4 cm/s. The observed variation in the Strouhal number indicates a maximum uncertainty of about 200 Hz between the coarsest and finest grids. This is considered satisfactory convergence. Therefore, all of the cases reported in this paper will use the $120 \times 104 \times 120$ grid.

Results and Discussion

We now present simulations of fully expanded supersonic jets at $M = 1.4$ with and without paddles immersed in the flow. Pitot pressure was chosen to provide a good qualitative picture of the jet mixing and motion. In particular, time series of pitot pressure plots for the jet with paddles are analyzed to show the flapping motion and its period. Although flow visualization can be enlightening about the overall flow, a more quantitative measure is required for frequency studies. Thus, the time histories of flow variables have been collected at various locations and then Fourier analyzed to provide a quantitative picture of the acoustic waves within the domain. We can quantitatively establish the connection between the flapping mode and the acoustic waves by studying the Fourier analyses of the local pressure and the z component of velocity w. We will also present some measures of the jet mixing and a discussion about the feedback mechanism and will close with some comparison to experimental data.

Jet Motion Visualization

To understand qualitatively the motion of a free jet and a jet with the paddles, we use the instantaneous pitot pressure distributions. The upper frame of Fig. 2 is the free jet and the lower frame is the jet with paddles. In both frames, the jet flows from left to right, and the nozzle is outlined on the left. In the bottom frame, the paddles are located in the middle. The pitot pressure used throughout this paper is obtained from a numerically simulated probe placed within the flow. It is corrected for the shock wave that would exist in front of a physical probe placed in a supersonic flow. From the figure, we see that instabilities develop along the edge of both jets and grow spatially moving from left to right. The jet without paddles shows a weak flapping motion and breaks up towards the end of the frame. The jet with

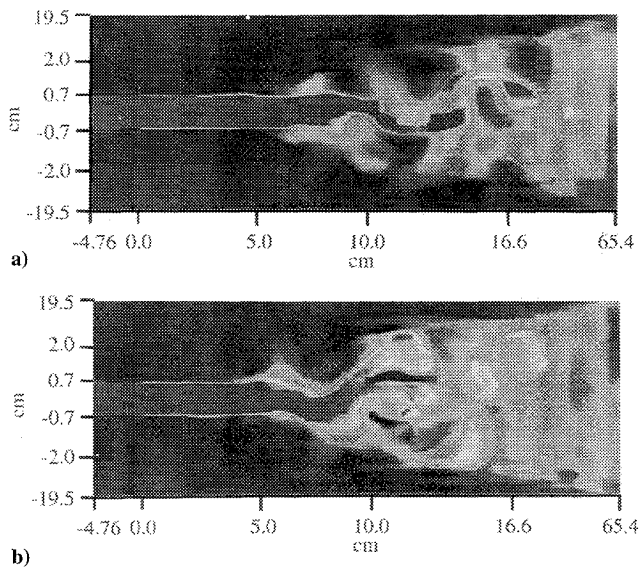

Fig. 2 Pitot pressure distribution shown in x–z plane at y = 0.0 cm, symmetry plane: a) without paddles and b) with paddles.

paddles becomes unstable closer to the nozzle, shows a more vigorous flapping motion, and is impacting the upper paddle at the time of this figure. After impacting the paddle, this jet quickly breaks up.

To visualize the flow modification caused by the paddles better and to understand the jet's flapping motion, Fig. 3 shows a time sequence of pitot pressure distributions (as seen from above) for a x–z plane located at $y = 0.0$ cm or the axis of symmetry. The time between frames was chosen to capture the periodic flapping mode in a minimum number of frames. Starting at the top frame of the figure, the jet is impacting the upper paddle and starting to move towards the lower paddle. The third frame, about halfway through the cycle, shows the jet breaking away from the lower paddle. The last frame, which is just a little past the completed cycle, shows that the jet has returned to a position similar to the first frame. From this sequence, the period for the flapping motion is estimated to be 0.00023 s or $St(h) = 0.126$. This is only a coarse estimate of the frequency, and in the next section Fourier analysis will be used to obtain a more quantitative value.

Frequency Analysis of Flow Variables

To determine the frequency content of acoustic fluctuations, we collected time histories of the flow variables at fixed locations in the computational domain and then Fourier analyzed these histories to determine the spectra. Since the previous figures illustrate that the dominant flow instability for the jet with paddles is the flapping mode in the minor axis, z direction, of the jet, the velocity fluctuations in the z direction, w, are Fourier analyzed and the resulting spectrum compared with the pressure fluctuation spectrum.

Figures 4 and 5 show the spectral (frequency–amplitude) relations revealed by the Fourier analysis of the z component of velocity and the local pressure at six locations downstream of the nozzle for the jet with paddles. Although the pressure fluctuations are more complex, being composed of the flow fluctuation in all directions, the same dominant frequencies seen in the z component of the velocity fluctuations are identified. These figures show many distinct frequencies that change from one location to another. However, for this configuration, the dominant frequency yields a Strouhal number $St(h)$ of 0.136. The spectrum analysis of the local pressure, in Fig. 5, represents the local sound levels. The 157.5-dB level for the dominant frequency near the nozzle, $x = 0.1$ cm, is in agreement with the experimental measurements of Rice and Raman.[7] Comparing this dominant frequency with the previously estimated flapping mode frequency obtained from the pitot pressure plots confirms that the flapping mode seen in the pitot pressure plots is the primary source of pressure fluctuations and the noise produced from this jet. We return to this analysis when we discuss the feedback mechanism.

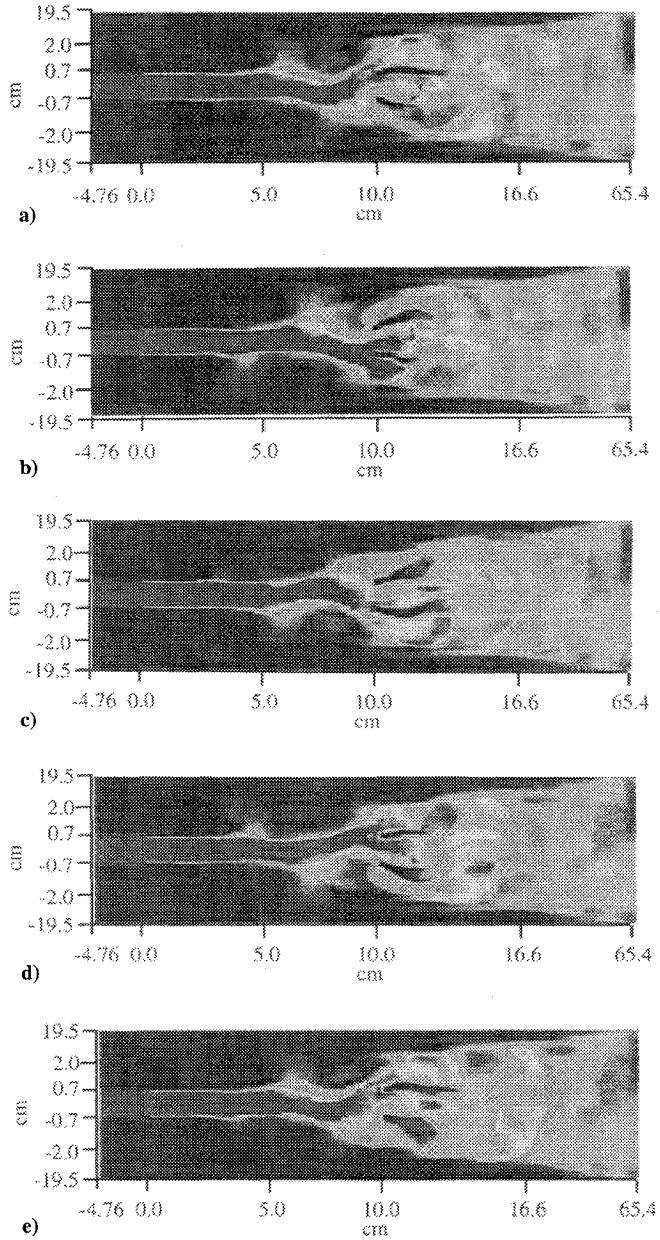

Fig. 3 Time sequence of pitot pressure distributions in the x–z plane at y = 0.0 cm at a) 0.0075 s, b) 0.00755 s, c) 0.00761 s, d) 0.00766 s, and e) 0.00773 s.

Similar Fourier analysis of the local pressure fluctuations and the z component of velocity fluctuations for the jet without paddles reveals a much less organized spectrum. Some of the same frequencies can be seen, but their amplitudes are smaller.

Jet Mixing

A measure of the jet mixing in experimental studies is the pitot or total pressure drop in the axial x direction.[7] Although the pitot pressure is not a linear function of the velocity, constant pitot pressure still represents a constant velocity with no mixing, and a decrease in pitot pressure represents a decrease in velocity and mixing with the surroundings. To model this measurement numerically, we have time averaged the pitot pressure along three lines parallel to the x axis (flow direction) at different values of y along the semimajor axis of the jet in the $z = 0.0$ cm plane. Figures 6 and 7 show the normalized pitot pressure vs the distance from the nozzle's lip (normalized by the nozzle's narrow dimension of 1.4 cm, h) for the cases without and with paddles, respectively. Each figure contains three lines, labeled pitot 1, located at $y = 0.025h$ or just off the jet's centerline; pitot 2, located at $y = 1.225h$ or about half the simulated nozzle's widest dimension; and pitot 3, located at $y = 2.48h$ or just

above the nozzle. As a point of reference, the paddles are located at a normalized distance of $7.8h$ in the simulation with paddles.

In Fig. 6, the case without paddles, pitot 1 and 2 show that the pitot pressure begins to decrease smoothly at approximately $6h$ downstream. We call this location the mixing inception point. The decrease in both curves continues from there, but neither quite reaches the surrounding pressure. Pitot 3, which starts at the background pressure, begins to increase at $2.5h$, reaches a peak at approximately $6h$ downstream, and then decreases. Again, it does not quite return to the surrounding pressure for the computational domain. Examining Fig. 7, the jet simulation with paddles, pitot 1 and 2, show that the pitot pressure begins to decrease before the paddles at about $4.5h$. Thus, the mixing inception point is earlier for the case with paddles than the case without paddles. Pitot pressure continues to drop along these lines until these lines reach the paddles where a local peak occurs. The pitot pressure along pitot 3 begins to rise at $2.5h$, peaks first at about $4h$, attains a second peak near the paddle location, and finally drops towards the background value. The pressure loss along pitot 1 and 2 before the paddles and the pressure gain along pitot 3 are caused by the flapping motion of the jet and resulting jet mixing. A local peak occurs along all three lines at the paddle location and is caused by the shock wave located just ahead of the paddles. Behind the paddles, the three curves show the pitot pressure continuing to drop to the surrounding pressure. The pitot pressure along pitot 1 shows the slowest recovery rate. This is not surprising since this line is located near the jet's center. At approximately $10h$ downstream of the paddles or $18h$ from the nozzle's lip, the average pitot pressure, along pitot 2 and 3, is within 20% of the surrounding pressure showing that the jet has dissipated into the surroundings. Thus, the pitot pressure plots indicate that the jet

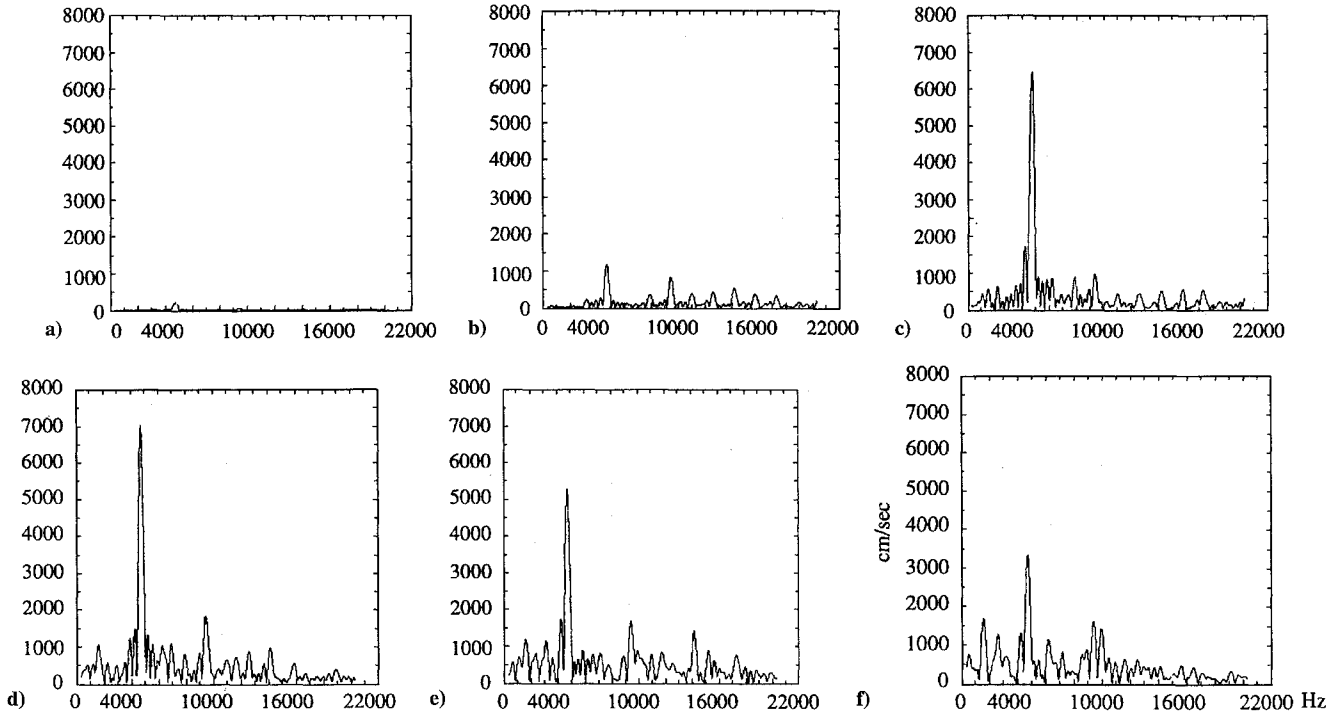

Fig. 4 Component of velocity fluctuations at $z = 0.475h$ and a) $x = 0.071h$, b) $x = 2.07h$, c) $x = 6.07h$, d) $x = 7.79h$, (e) $x = 9.1h$, and f) $x = 11.1h$.

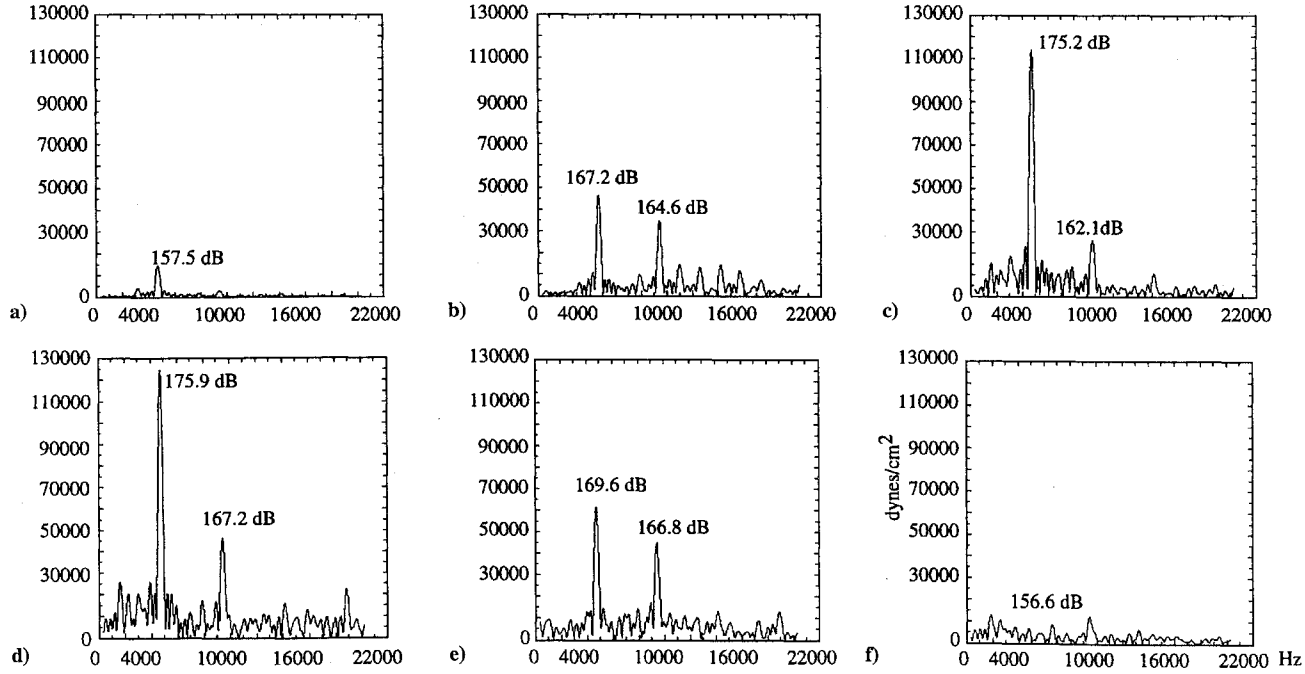

Fig. 5 Pressure fluctuations at $z = 0.475h$ and a) $x = 0.071h$, b) $x = 2.07h$, c) $x = 6.1h$, d) $x = 7.79h$, e) $x = 9.1h$, and f) $x = 11.1h$.

Table 1 Flux ratio (the flux through the plane divided by the nozzle's exit flux) through constant x planes located at various positions down the jet

Position, cm	X momentum and mass flux ratio through planes			
	Without paddles		With paddles	
	Momentum	Mass	Momentum	Mass
0.0	1.00	1.00	1.00	1.00
0.0	1.00	1.34	1.00	1.40
11.4	1.07	2.02	1.09	2.16
13.3	1.08	2.23	0.89	2.36
17.7	1.09	2.57	0.88	2.62

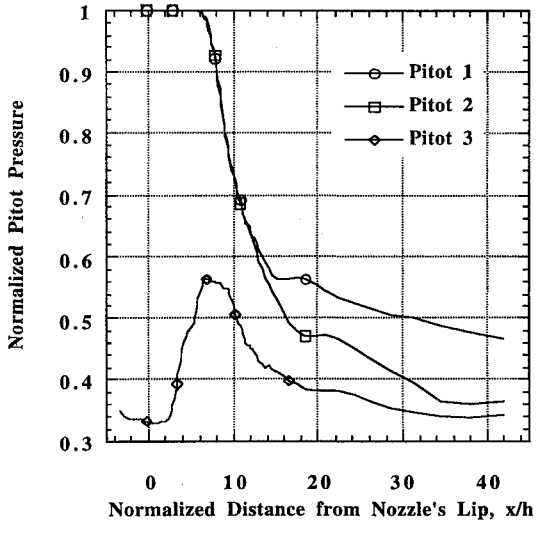

Fig. 6 Streamwise variation of the average pitot pressure at three locations in the jet without paddles.

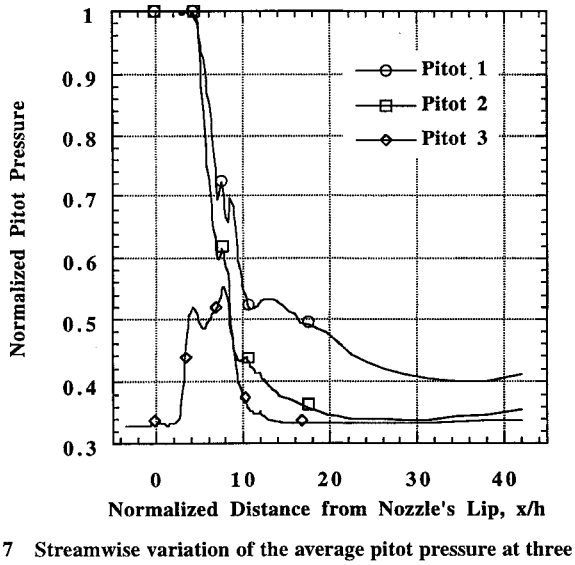

Fig. 7 Streamwise variation of the average pitot pressure at three locations in the jet with paddles.

exhaust in the simulation without paddles has not dissipated at this point, whereas it has dissipated for the case with paddles.

An additional method of measuring the jet's mixing is by determining the mass and momentum fluxes through planes perpendicular to the jet flow. To model this measurement numerically, we have time averaged the mass and x-momentum flux through five cross sections located at various x locations. Table 1 contains the flux data normalized by the nozzle's exit flux for the jet without and with paddles. All planes, except the first plane, extend to the computational domain boundaries in the y and z directions. Therefore, the fluxes through these planes include mass and momentum drawn into the computational domain through the boundaries. The first plane, located at the nozzle exit, has been confined to the height and width of

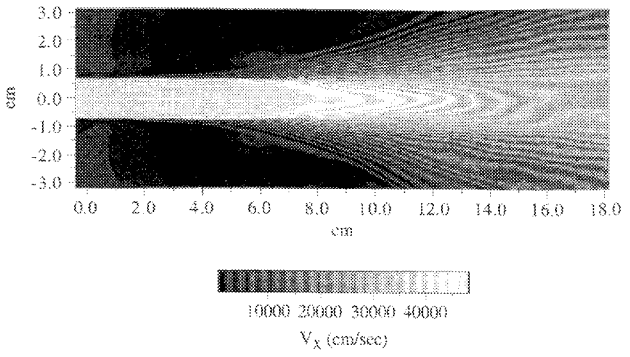

Fig. 8 Time average x component of velocity for a jet without paddles at $y = 0.0$ cm, symmetry plane.

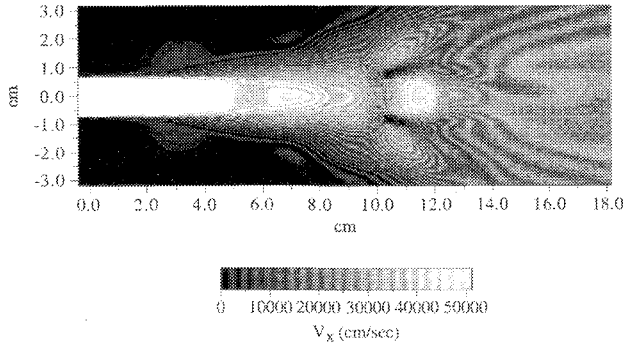

Fig. 9 Time average x component of velocity for a jet with paddles at $y = 0.0$ cm, symmetry plane.

the nozzle, and therefore these average values should represent the correct nozzle outflow. The jump in integrated x momentum and mass between the first two planes in the table occurs because of the additional mass and x momentum contained in the surrounding fluid. Without the paddles, the x momentum increases down the jet, and the mass flux also increases down the jet. With the paddles, the x momentum appears to peak just after the paddles and then decreases. Comparing the x-momentum flux at the last two locations shows that the integrated x momentum for the case with paddles is much lower than the momentum of the jet without the paddles. Comparing the mass flux for the locations after the exit planes shows mass flux for the jet with paddles having a slightly larger value than mass flux for the jet without paddles. These data indicate that the paddles have caused the jet to mix better with its surroundings.

Time average values of the x component of velocity, u or V_x, pitot pressure, and Mach number have also been analyzed to determine the jet mixing and the effects of the paddles on the flow. These averages are over 5000 time steps or for 2.5×10^{-3} s. Since the plots from these three quantities are very similar, only the x component of velocity will be presented. Figures 8 and 9 are plots of the x component of velocity at the plane of symmetry, $y = 0.0$ cm, for the jets without and with paddles. Again, as with previous figures, the flow is from left to right. In these figures, the jets can be seen expanding initially at approximately 10 deg as they mix with the surrounding fluid. The jet with paddles shows the jet's expansion angle increasing to approximately 20 deg (Fig. 9). Also, the mixing inception point clearly occurs earlier for the jet with paddles. Figure 9 also clearly shows the wake regions behind the paddles and the compression zone in front of the paddles. A supersonic region exists downstream of the paddles and along the centerline. This region is caused by the paddles acting like a converging-diverging nozzle with the flow expanding in the z direction as it flows downstream in the x direction.

Drag and Thrust Loss

We have also estimated the drag forces on the paddles and thrust loss using our numerical simulations. A control volume surrounding the paddles was chosen. We numerically integrated the fluxes passing through the faces of and within the control volume and the

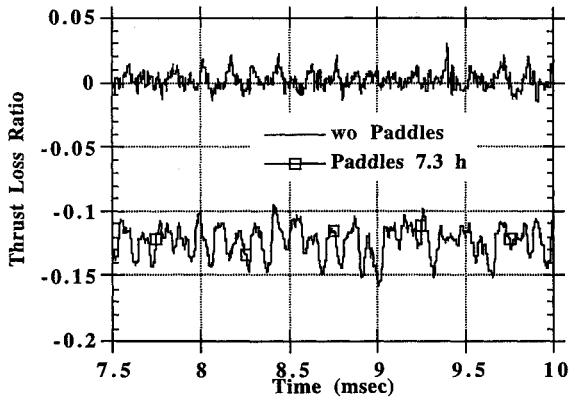

Fig. 10 Thrust loss ratio without and with paddles.

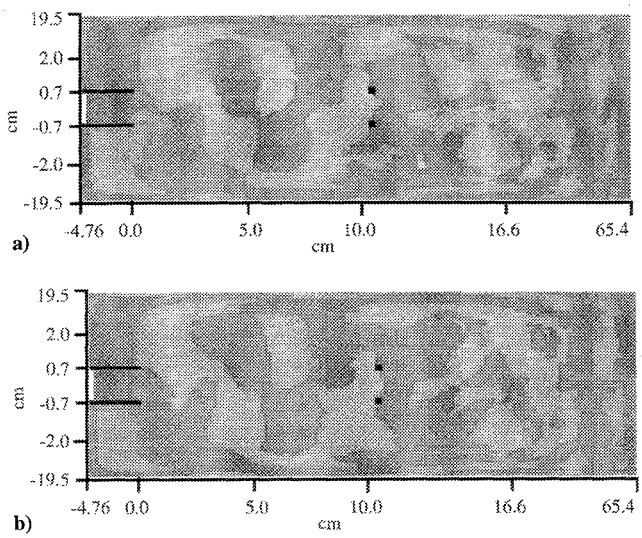

Fig. 11 Time sequence of special local pressure distributions in the x–z plane at a) 0.008376 s and b) 0.008388 s.

pressure acting on the control volume to predict the drag forces acting on the paddles in the x, y, and z directions. For the thrust loss, the pressure forces in the x direction and the x-momentum fluxes through the six control surfaces and the x momentum's time rate of change within the control volume were evaluated to estimate the drag force in the x direction. Figure 10 shows the thrust loss ratio determined for a jet without paddles and with paddles at $7.3h$ from the nozzle. The average thrust loss ratio for the simulation without paddles should be zero as shown in the figure. This result gives us some confidence in the drag force evaluation from our numerical simulation. Our estimated thrust loss ratio for the case with the paddles present is 13%. Raman and Rice[17] obtained a drag loss value of 14.4% in their experiment. In their experimental setup, there are paddle supports not included in our simulation, probably bringing the experimental and simulated values even closer.

Feedback Mechanism

In the Introduction, a feedback mechanism was suggested in which the paddles generate an impingement tone that propagates upstream in the periphery of the jet and excites the flapping mode. It is difficult to isolate these acoustic waves numerically. Large flow perturbations are present, and the resulting pressure fluctuations that dominate the region between the nozzle and the paddles also contain the pressure signatures of the time-varying vorticity. We have generated some special local pressure distribution plots to try to isolate these feedback waves at least in the region close to the nozzle. We compress the large peaks and highlight the small acoustic waves using an ad hoc procedure. First the background pressure was subtracted from the local pressure. If the resulting difference was greater than 1 dyne/cm^2, the natural log was taken. If the difference was less than -1 dyne/cm^2, the natural log was taken of the absolute values and given a negative sign. If the difference was between -1 and

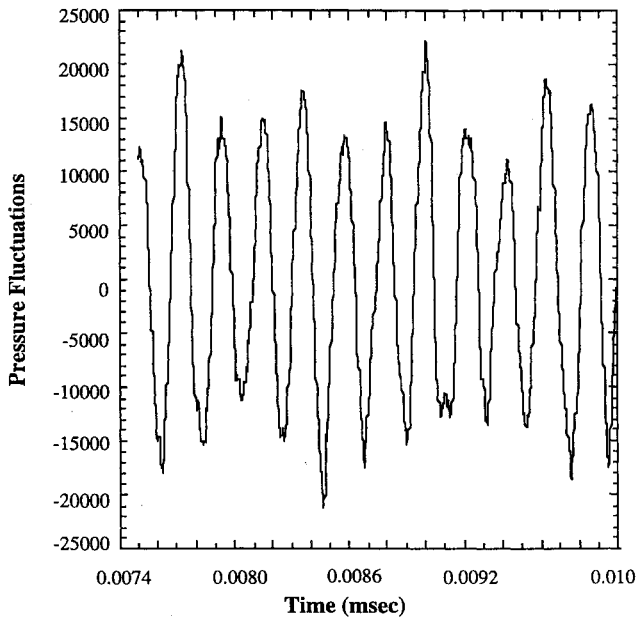

Fig. 12 Pressure fluctuations at $x = 1.36h$.

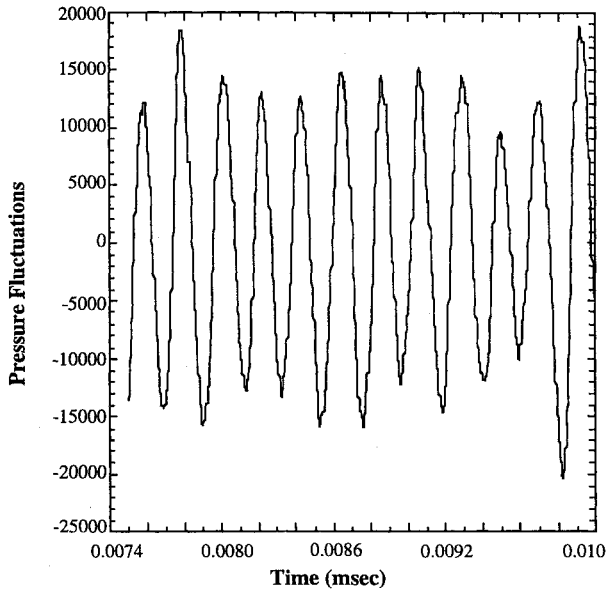

Fig. 13 Pressure fluctuations at $x = 0.071h$.

$+1$ dyne/cm^2, a value of zero was assigned. Figure 11 shows the resulting pressure distribution plot seen from above for two different time steps for the case with the paddles at $7.3h$. The upper frame shows the edge of a pressure wave to the upper right of the nozzle. In the next frame, this wave has contacted the nozzle's lip showing that the wave is moving from right to left.

Figures 12 and 13 show the time history of the local pressure minus the local average pressure over the period shown. Figure 12 is located at $x = 1.36h$, and Fig. 13 is located at $x = 0.071h$; both are at same height above the nozzle at $y = 2.47h$ and beyond the nozzle edge at $z = 0.97h$. From these two figures, one can see the fluctuations in Fig. 12 are leading in time by approximately 0.00005 s the same fluctuations in Fig. 13. This is as expected for waves traveling upstream towards the nozzle. The estimated rate of propagation from this data is 360.0 m/s, which for the accuracy of the time estimate is in very good agreement with the expected value for the speed of sound.

Summary and Conclusions

The acoustic noise and mixing of jets are usually studied experimentally or analytically. To simulate a jet and predict its noise numerically, the fluid dynamics and encapsulated acoustic wave

equations must be modeled and captured by the computational domain and method. In our present work, the FAST3D program using the FCT algorithms and the VCE technique have been used to simulate a supersonic rectangular jet with and without flow modifiers, called paddles.

We have shown, using pitot pressure plots, that the addition of the paddles strengthens a periodic flapping mode in the minor axis direction. Fourier analysis of the fluctuation in local pressure and the z component of the velocity near the paddles shows that the flapping mode $St(h)$ is approximately 0.136. A similar Fourier analysis for the free jet does not show a dominant frequency but shows multiple frequency peaks.

Using time-averaged pitot pressures, we have shown that the addition of paddles increases jet mixing when compared with a case without paddles. In the case presented, the paddles, located downstream of the mixing inception point for the jet without paddles, moves the inception point closer to the nozzle's exit plane. The mixing inception point is defined here as the location where the pitot pressure begins to drop. For the jet with paddles, the pitot pressure reaches the surrounding pressure levels quickly, whereas for the jet without paddles the pitot pressure does not reach the surrounding pressure levels within the computational domain used. This indicates that the jet with paddles has essentially dissipated within the computational domain, whereas the jet without paddles has not dissipated. In addition, the time average plots of the x component of velocity for the jet with paddles also show that the mixing inception point moves towards the nozzle and the angle of expansion increases compared with the jet without paddles.

From the numerical simulations, the thrust loss caused by the paddles is estimated to be about 13%, which is in agreement with the experimentally determined value of 14.4%, considering that the support for the paddles is not included in the simulations. The amplitude and frequency of the flapping motion are also in good agreement with experimental data.

Acoustic waves at the dominant frequency have been identified to move from the paddles to the lip of the nozzle, thus establishing a feedback loop. It therefore appears possible to control the frequency and mixing by varying the location and immersion of the paddles. The thrust loss needs to be reduced with the use of more aerodynamic shapes for the paddles before such a concept can be used in a practical device. Initial experimental research has been performed by Raman and Rice[18] on this issue.

Acknowledgments

This work was partially supported by the Internal Fluid Mechanics Division of the NASA Lewis Research Center and by the 6.1 Computational Physics Task Area of the Naval Research Laboratory. The FAST3D program development has been partially supported by the Advanced Research Projects Agency, Advanced Computational Mathematics Program. This work was also supported in part by a grant of high-performance computing time from the Department of Defense HPC Shared Resource Center Wright Laboratory's Paragon.

References

[1]Drummond, J. P., "Supersonic Reacting Internal Flow Fields," *Numerical Approaches to Combustion Modeling*, Vol. 135, Progress in Astronautics and Aeronautics, AIAA, Washington, DC, 1991, pp. 365–420.

[2]Li, C., Kailasanath, K., and Book, D. L., "Mixing Enhancement by Expansion Waves in Supersonic Flows of Different Densities," *Physics of Fluids A*, Vol. 3, No. 5, 1991, pp. 1369–1373.

[3]Lepicovsky, J., Ahuja, K. K., Brown, W. H., and Burring, R. H., "Coherent Large-Scale Structures in High Reynolds Number Supersonic Jets," *AIAA Journal*, Vol. 25, No. 11, 1987, pp. 1419–1425.

[4]Ahuja, K. K., and Brown, W. H., "Shear Flow Control by Mechanical Tabs," AIAA Paper 89-0994, Jan. 1989.

[5]Zaman, K. B. M. Q., Reeder, M. F., and Samimy, M., "Control of an Axisymmetric Jet Using Vortex Generators," *Physics of Fluids*, Vol. 6, No. 2, 1994, pp. 778–793.

[6]Strykowski, P. J., Krothapalli, A., and Wishart, D., "The Enhancement of Mixing in High Speed Heated Jets Using a Counterflowing Nozzle," AIAA Paper 92-3262, July 1992.

[7]Rice, E. J., and Raman, G., "Enhanced Mixing of a Rectangular Supersonic Jet by Natural and Induced Screech," AIAA Paper 93-3263, July 1993.

[8]Lighthill, M. J., "Jet Noise," *AIAA Journal*, Vol. 1, No. 7, 1963, pp. 1507–1517.

[9]Powell, A., Umeda, Y., and Ishii, R., "Observations of the Oscillation Models of Choked Circular Jets," *Journal of the Acoustical Society of America*, Vol. 95, No. 5, 1992, pp. 2823–2836.

[10]Tam, C. K. W., "Excitation of Instability Waves in a Two-Dimensional Shear Layer by Sound," *Journal of Fluid Mechanics*, Vol. 89, Pt. 2, 1978, pp. 357–371.

[11]Tam, C. K. W., and Ahuja, K. K., "Theoretical Model of Discrete Tone Generation by Impinging Jets," *Journal of Fluid Mechanics*, Vol. 214, May 1990, pp. 67–87.

[12]Boris, J. P., and Book, D. L., "Flux-Corrected Transport I: SHASTA, A Fluid Transport Algorithm That Works," *Journal of Computational Physics*, Vol. 11, No. 1, 1973, pp. 38–69; also see "Solution of the Continuity Equation by the Method of Flux-Corrected Transport," *Methods in Computational Physics*, Academic, New York, 1976, pp. 85–129.

[13]Boris, J. P., Landsberg, A. M., Oran, E. S., and Gardner, J. H., "LCPFCT—A Flux-Corrected Transport Algorithm for Solving Generalized Continuity Equations," Naval Research Lab., NRL Memorandum Rept. 6410-93-7192, Washington, DC, April 1993.

[14]Landsberg, A. M., Young, T. R., and Scott, R. J., "Computing Shocked Flows Through the Euler Equations," *Proceeding of the 19th International Symposium on Shock Waves*, Shock Waves @ Marseille I, edited by R. Brum and L. Z. Dumitrescu, Springer–Verlag, Germany, 1995, pp. 421–426.

[15]Landsberg, A. M., Young, T. R., Jr., and Boris, J. P., "An Efficient, Parallel Method for Solving Flows in Complex Three-Dimensional Geometries," AIAA Paper 94-0413, Jan. 1994.

[16]Young, T. R., Jr., Landsberg, A. M., and Boris, J. P., "Implementation of the Full 3D FAST3D (FCT) Code Including Complex Geometry on the Intel iPSC/860 Parallel Computer," *Proceedings from High Performance Computing 1993: Grand Challenges in Computer Simulation*, Society for Computer Simulation, San Diego, CA, 1993, pp. 143–148.

[17]Raman, G., and Rice, E. J., "Mixing and Noise Benefit Versus Thrust Penalty in Supersonic Jets Using Impingement Tones," AIAA Paper 94-2955, June 1994.

[18]Raman, G., and Rice, E. J., "Supersonic Jet Mixing Enhancement Using Impingement Tones from Obstacles of Various Geometries," *AIAA Journal*, Vol. 33, No. 3, 1995, pp. 454–462.